Photon gating in four-dimensional ultrafast electron microscopy

Mohammed T. Hassan, Haihua Liu, John Spencer Baskin, and Ahmed H. Zewail[1]

Physical Biology Center for Ultrafast Science and Technology, Arthur Amos Noyes Laboratory of Chemical Physics, California Institute of Technology, Pasadena, CA 91125

Contributed by Ahmed H. Zewail, September 9, 2015 (sent for review August 24, 2015; reviewed by Andrea Cavalleri and Chong-Yu Ruan)

Ultrafast electron microscopy (UEM) is a pivotal tool for imaging of nanoscale structural dynamics with subparticle resolution on the time scale of atomic motion. Photon-induced near-field electron microscopy (PINEM), a key UEM technique, involves the detection of electrons that have gained energy from a femtosecond optical pulse via photon–electron coupling on nanostructures. PINEM has been applied in various fields of study, from materials science to biological imaging, exploiting the unique spatial, energy, and temporal characteristics of the PINEM electrons gained by interaction with a "single" light pulse. The further potential of photon-gated PINEM electrons in probing ultrafast dynamics of matter and the optical gating of electrons by invoking a "second" optical pulse has previously been proposed and examined theoretically in our group. Here, we experimentally demonstrate this photon-gating technique, and, through diffraction, visualize the phase transition dynamics in vanadium dioxide nanoparticles. With optical gating of PINEM electrons, imaging temporal resolution was improved by a factor of 3 or better, being limited only by the optical pulse widths. This work enables the combination of the high spatial resolution of electron microscopy and the ultrafast temporal response of the optical pulses, which provides a promising approach to attain the resolution of few femtoseconds and attoseconds in UEM.

photon-induced near-field electron microscopy | attosecond electron microscopy | optical-gated electron pulse | time-resolved PINEM | photon–electron gating

In ultrafast electron microscopy (UEM) (1–3), electrons generated by photoemission at the cathode of a transmission electron microscope are accelerated down the microscope column to probe the dynamic evolution of a specimen initiated by an ultrafast light pulse. The use of femtosecond lasers to generate the electron probe and excite the specimen has made it possible to achieve temporal resolution on the femtosecond time scale, as determined by the cross-correlation of the optical and electron pulses. One important method in the UEM repertoire is photon-induced near-field electron microscopy (PINEM) (4, 5), in which the dynamic response detected by the electron probe is the pump-induced charge density redistribution in nanoscale specimens (6).

Photon–electron coupling is the basic building block of PINEM, which takes place in the presence of nanostructures when the energy-momentum conservation condition is satisfied (4, 5). This coupling leads to inelastic gain/loss of photon quanta by electrons in the electron packet, which can be resolved in the electron energy spectrum (5, 7, 8). This spectrum consists of discrete peaks, spectrally separated by multiples of the photon energy ($n\hbar\omega$), on the higher and lower energy sides of the zero loss peak (ZLP) (4) (Fig. 1). The development of PINEM enables the visualization of the spatiotemporal dielectric response of nanostructures (9), visualization of plasmonic fields (4, 5) and their spatial interferences (10), imaging of low atomic number nanoscale materials (11), characterization of ultrashort electron packets (12, 13), and imaging of different biological structures (14).

As shown by Park et al. (5), the PINEM intensity (I_{PINEM}) is given by the square modulus of the field integral $\tilde{F}_0$ (i.e., $I_{PINEM} \propto |\tilde{F}_0|^2$), in the weak interaction limit. The near field of a nanoparticle leads to the scattering of the electron packet, which can be treated rigorously using the Schrödinger equation/Mie scattering theory. It follows that PINEM images the object and displays its field characteristics depending on its shape, the polarization and wavelength of optical excitation, and the width of pulses used. For a spherical nanoparticle, the field integral at point (x, y) in the specimen plane is simplified to give (6)

$$\tilde{F}_0 \approx -i\tilde{E}_0 \cos\phi\chi_s \frac{2}{3} a^3 (\Delta k)^2 K[\Delta k b], \quad [1]$$

where $\tilde{E}_0$ is the electric field amplitude of the incident light, ϕ the light polarization angle, a the particle radius, $b = \sqrt{x^2+y^2}$ the impact parameter, K the modified Bessel function of the second type, Δk the momentum change of the electron, and $\chi_s = 3(\varepsilon-1)/(\varepsilon+2)$, where χ_s is the material susceptibility and ε the dielectric function.

In previous studies of the parameters in Eq. **1**, only $\tilde{E}_0$ was time dependent. The PINEM intensity, at a given point in space, was a function only of the time delay between the optical and electron pulses, providing, for the pulse lengths currently used, a cross-correlation profile when this delay was scanned across the time of temporal coincidence, or $t = 0$ (4, 5, 9, 13). Hitherto, PINEM has not been used to study the ultrafast dynamics of matter. Here, we follow the strategy of using the PINEM gain electrons generated by a first optical pulse, whose delay relative to the electron pulse is maintained at $t = 0$, to probe dynamics initiated by introduction of a second optical pulse on the specimen, as proposed theoretically in ref. 15. By this approach, we were able to optically gate the electron pulse (i.e., create an electron pulse that only lasts for the duration of the optical pulse)

Significance

In this contribution, we demonstrate a unique concept in the use of photon-induced near-field electron microscopy—combining one electron pulse and two optical pulses—as a probe for ultrafast dynamics of matter in electron microscopy. Photon–electron coupling permits the use of a short optical pulse to gate the electron pulse, which is serving as a probe of the ultrafast dynamics triggered by another optical pulse. This technique provides the high spatial and temporal resolution of the electron pulse and optical laser pulses, respectively, both in ultrafast electron microscopy (UEM) measurements. This development paves the way for numerous studies in imaging of matter not only with few femtosecond resolution but also with the potential for attosecond imaging in UEM.

Author contributions: M.T.H., H.L., J.S.B., and A.H.Z. designed research, performed research, contributed new reagents/analytic tools, analyzed data, and wrote the paper.

Reviewers: A.C., Max Planck Institute; and C.-Y.R., Michigan State University.

The authors declare no conflict of interest.

Freely available online through the PNAS open access option.

[1]To whom correspondence should be addressed. Email: zewail@caltech.edu.

This article contains supporting information online at www.pnas.org/lookup/suppl/doi:10.1073/pnas.1517942112/-/DCSupplemental.

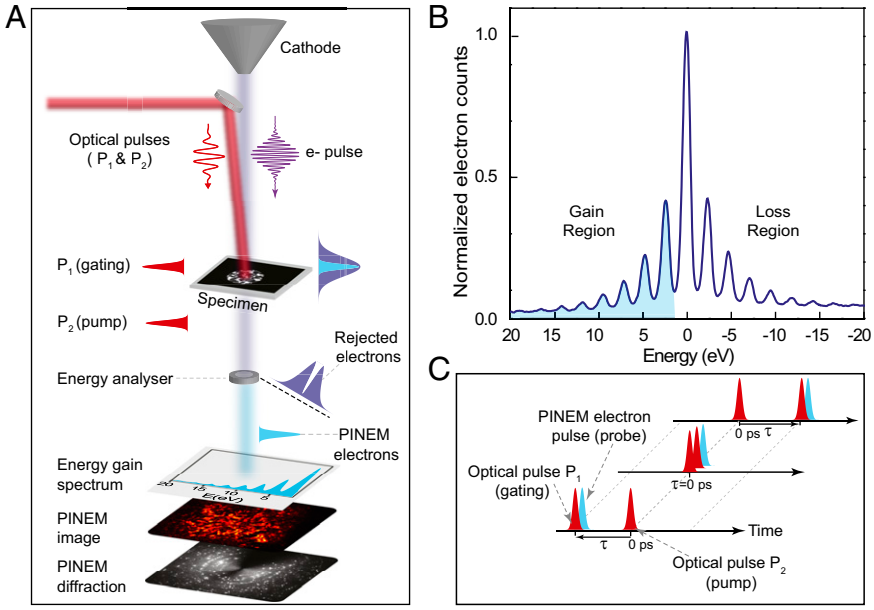

Fig. 1. Concept of photon gating in 4D electron microscopy. (*A*) The microscope column with one electron (dark blue) and two optical (red) pulses focused onto the specimen. The wavefunctions of the three pulses are schematically shown at the top. One optical pulse is coincident with the electron pulse at the specimen to generate a PINEM signal. The resulting light blue PINEM pulse is sliced out from other electrons for detection as an energy spectrum, an image, or a diffraction signal (see the text). The second optical pulse initiates the dynamics to be probed. (*B*) Electron energy spectrum generated at the specimen plane when optical and electron pulses arrive simultaneously. The gain energy range is shaded light blue. (*C*) Illustration for the temporal pulse sequence, two optical and one electron pulse for ultrafast time-resolved PINEM measurements.

and achieve significant enhancement of the temporal resolution (see the second paragraph below).

The concept of the experiment is illustrated by Fig. 1*A*, in which the electron pulse in blue and one optical pulse (P_1) in red are shown arriving at the specimen plane simultaneously. Interaction between photon and electron in the presence of the specimen "slices out" the light blue pulse of gain electrons, which are separated from all other electrons by energy dispersion or

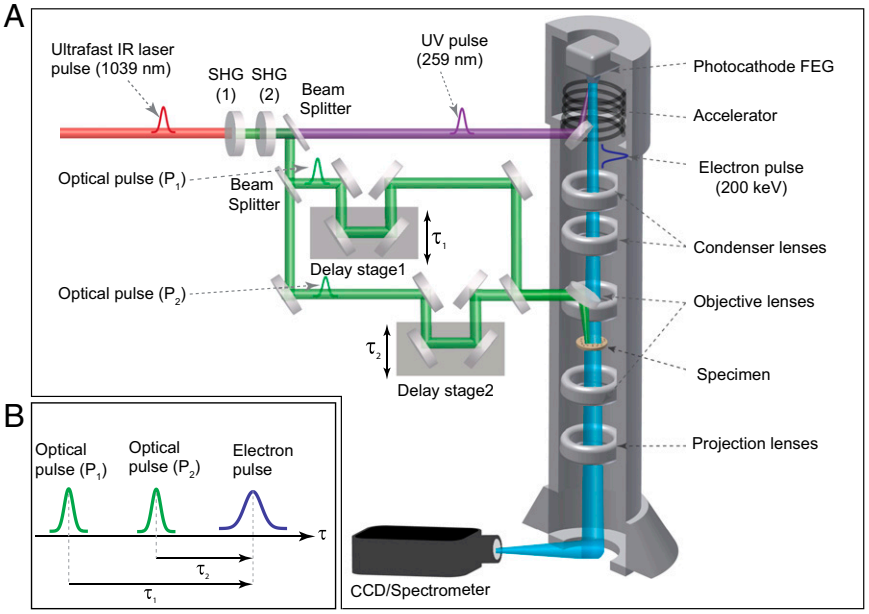

Fig. 2. Experimental arrangement of optical gating in UEM. (*A*) IR 300 ± 50-fs laser pulses ($\lambda \sim 1{,}039$ nm) are frequency doubled to generate visible laser pulses (~519 nm). UV laser pulses ($\lambda \sim 259$ nm) are obtained by a second harmonic generation of the visible laser pulses and directed to the photoemissive cathode inside the microscope to generate ultrafast electron pulses. The visible laser beam is divided into two optical pulse trains. The delays between the two optical pulses and electron pulse (τ_1, τ_2) are controlled by linear delay stages. These optical pulses are recombined and focused onto the specimen in the microscope and the electron energy spectrum is acquired by electron energy spectrometer. (*B*) Time axis showing passage of pulses through the specimen plane and the delays (τ_1, τ_2) between the pulses.

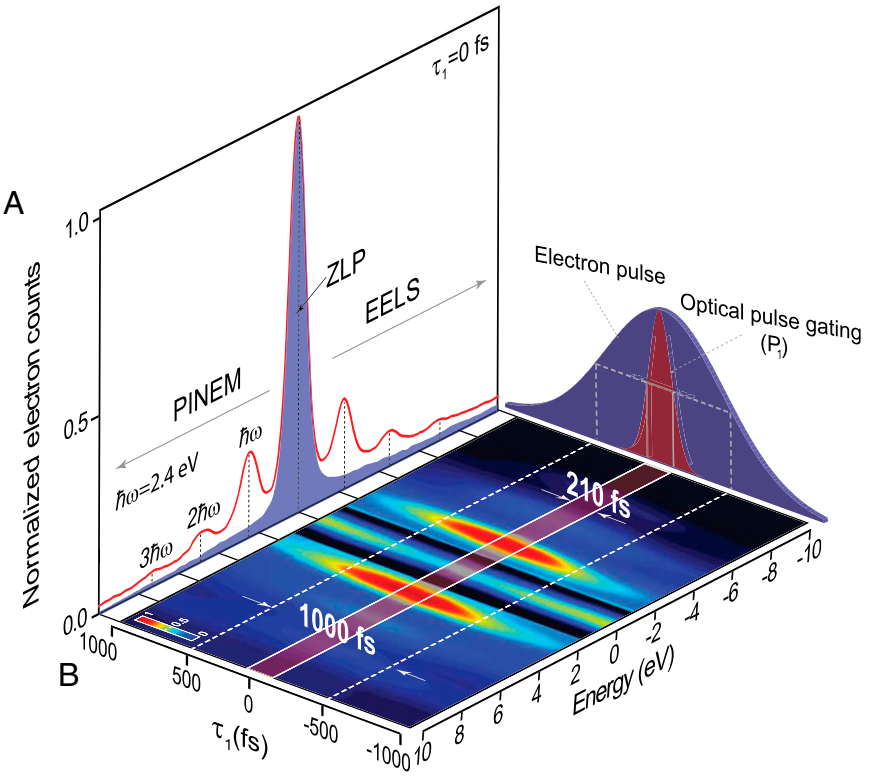

Fig. 3. Ultrafast optical gating and PINEM of vanadium dioxide nanoparticles. (*A*) PINEM spectrum at τ_1= 0 fs, which consists of discrete peaks on the higher and lower energy sides of the ZLP separated by multiple photon-energy quanta (~2.4 eV). The shaded curve presents the normalized ZLP measured at τ_1 = 1,000 fs. (*B*) PINEM spectrogram of photon–electron coupling of the first optical and electron pulse as a function of the first optical pulse delay (τ_1). The ZLP area between −1.5 and 1.5 eV has been reduced for visualization of the adjacent discrete peaks. Optical gating is clearly manifested in the narrow red strip corresponding to the width of the optical pulse (210 ± 35 fs; see *Results and Discussion*) shown in red in the vertical plane on the right, which is superimposed on the ultrafast electron pulse (1,000 fs) in blue.

filtering to be detected according to microscope settings in spectroscopy, imaging, or diffraction mode, as illustrated schematically at the bottom of the column. Note, it is possible to obtain PINEM diffraction, but this is not the subject of this paper. A second, or pump, optical pulse (P_2) is shown below the specimen, having already triggered the dynamics of interest. A series of time axes is plotted in Fig. 1*C* showing examples of characteristic sequences of pulse arrival times at the specimen plane during the experiment, with the pump arrival defining the zero of time.

A striking feature of this technique that was alluded to above is the potential for high temporal resolution, unlimited by the electron pulse duration, because the optical pulse acts as a temporal gate for a longer electron pulse. In the weak interaction limit, the duration of the pulse of PINEM electrons emulates that of the optical pulse that created it (15), as clearly shown in Fig. 1*A*. When these photon-gated electrons are used to probe dynamics triggered by a second ultrafast optical pulse, the time resolution is determined by the cross-correlation of the two optical pulses. This paves the way for the realization of attosecond electron microscopy, as done in all-optical spectroscopy (16) but with the spatial resolution being that of atomic motions. As suggested in Fig. 1*A*, we envisage the use of the photon-gated electron pulses, in imaging or in diffraction mode, for the study of a variety of optically initiated material processes, either of the nanostructure or of its surrounding media.

The PINEM signal can be directly monitored to detect changes in any of the specimen optical or physical properties expressed in Eq. **1**. Here, we demonstrate the use of the time-resolved PINEM technique where it is shown that the photoinduced dielectric response of VO_2—which is strongly related to the lattice symmetry (17)—manifests itself in a change in PINEM intensity. We relate the changes in optical properties of the polycrystalline VO_2 nanoparticles to the phase transition dynamics from initial (monoclinic) insulator phase to (tetragonal) metal phase, the subject of numerous previous studies.

Vanadium dioxide has been discussed as an active metamaterial (18) and one of the best candidates for solid-state ultrafast optical switches in photonics applications (19, 20) due to its unique structural photoinduced phase transition behavior (21). This phase transition has been examined by investigating the change in the heat capacity through thermal excitation (22, 23), whereas its ultrafast dynamics has been studied by optical spectroscopy (24, 25), THz spectroscopy (26, 27), X-ray diffraction (28, 29), ultrafast electron crystallography (30), and electron microscopy (31).

Experiment and Methods

In our experimental setup, as shown in Fig. 2*A*, infrared (300 ± 50 fs) laser pulses (λ ~ 1,039 nm, 100-kHz repetition rate) were frequency doubled and visible laser pulses with photon energy ($\hbar\omega$) ~2.4 eV were generated. The visible laser beam propagates through a second harmonic generation crystal to generate UV laser pulses (~259 nm). These UV pulses were directed to the photoemissive cathode to generate ultrafast electron pulses, which are accelerated (200 keV) in the electron microscope column. The microscope is equipped with an electron energy spectrometer for measurements of the electron energy spectrum of the electron pulses after their passage through the specimen. The experiment is conducted in the single-electron regime (2, 32) to reduce the space-charge effect and to attain high electron spectral and temporal resolutions. The visible laser beam was divided by another beamsplitter into two optical laser pulses P_1 and P_2. The delays (τ_1, τ_2) between (P_1, P_2) and the electron pulse are controlled by two linear stages. Later, these two optical pulses P_1 and P_2 were recombined and focused onto

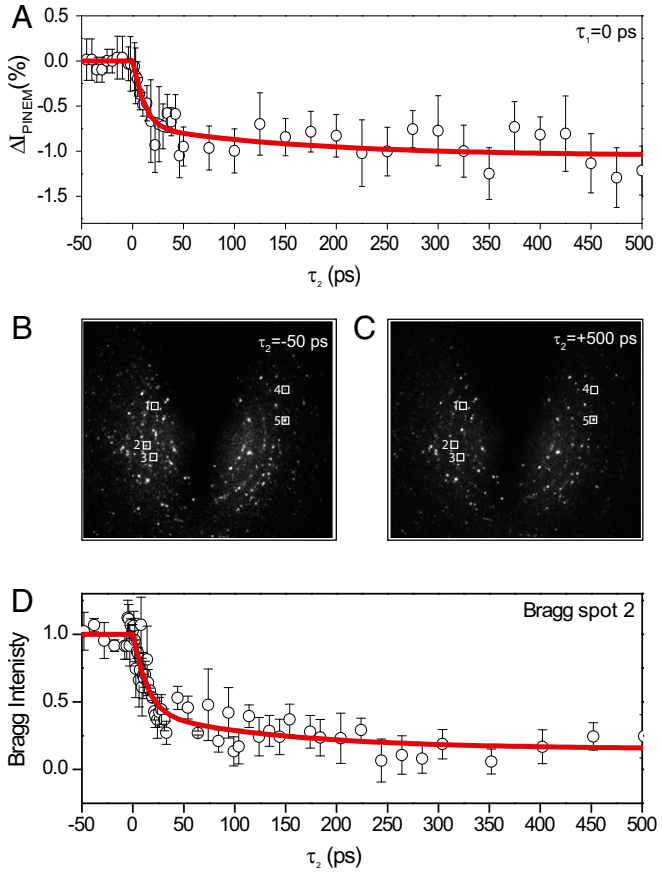

Fig. 4. Phase transition in vanadium dioxide nanoparticles. (*A*) The change of the PINEM spectrum intensity, which is obtained by the coupling between the first optical (P_1) and electron pulses onto the nanoparticles, as a function of the second optical pulse (pump) delay (τ_2), where the data points present the integration of the PINEM spectrum shown in Fig. 3*A* at time (τ_2). This dynamics curve represents the average of 10 data sets recorded under identical conditions. The biexponential fitting is shown in the red line. (*B* and *C*) Electron diffraction patterns of the same sample at two different delay times $\tau_2 = -50$ ps, and +500 ps, respectively. The diffraction pattern at $\tau_2 = -50$ ps in *B* shows Bragg spots (1–4) which are assigned to the monoclinic (low-temperature) phase of VO_2 (35). At $\tau_2 = +500$ ps, these Bragg spots disappear after the pump pulse as shown in *C*, which indicates the phase transition to the tetragonal (rutile) phase. The Bragg spot 5 in *B* and *C* belongs to the graphene substrate, and shows no change at the two delay times. (*D*) The decay in the Bragg spot 2 intensity as a function of the pump laser pulse delay time (τ_2). The biexponential fit is presented by the red line.

the specimen inside the microscope. The general case of arbitrary times of arrival of the two optical pulses at the specimen relative to that of the electron pulses is illustrated on the time axis of Fig. 2*B*.

Results and Discussion

In preparation for the pump-probe PINEM experiments, the first optical pulse (P_1), with fluence of 1.3 mJ/cm^2, was directed onto the specimen of VO_2 nanoparticles (diameter ~200 nm; see *Supporting Information*, *section S1*, Fig. S1*A*) and the electron energy spectrum was measured as a function of time delay (τ_1) to determine the temporal overlap at which the PINEM coupling is maximized ($\tau_1 = 0$ fs). The acquired "PINEM spectrogram" is shown in Fig. 3*B*. At $\tau_1 = 0$ fs, the electron energy spectrum (red line, Fig. 3*A*) carries the signature of photon–electron coupling. It consists of discrete peaks at integer multiples of the 2.4-eV photons on both sides of the ZLP, which is shown as a shaded area in Fig. 3*A*, measured at $\tau_1 = 1{,}000$ fs. The PINEM image of the sample can be obtained by energy filtering of the electrons that have only gained photon quanta (*Supporting Information*, *section S1*, Fig. S1*B*).

Henceforth, the first optical (gating) pulse (P_1) is preserved at spatiotemporal overlap ($\tau_1 = 0$ fs). Then, the second optical pulse (P_2) (pump pulse), with fluence 5.7 mJ/cm^2, has been used to induce the phase transition in the VO_2 nanoparticles. The PINEM spectrum, generated by the coupling of P_1 and electron pulses (Fig. 3*A*), was measured as a function of the second optical (pump) pulse delay (τ_2). The change of the PINEM spectrum intensity due to the photoinduced insulator–metal phase transition is traced and shown in Fig. 4*A*, where the data points present the integration of the PINEM spectrum at each delay time (τ_2). The data points acquired from $\tau_2 = -1$ to 1 ps have been excluded due to the contribution of the PINEM spectrum generated by the coupling of the second optical pulse (P_2) and the electron pulse, which is not relevant to the phase transition measurement.

Additional tests of gating were made by replacing P_2 with a 3.6-eV UV pulse. Consistent with the expected gating, we detected a new PINEM band at 6 eV, which is the sum of the P_1 and UV photon energies, indicating that P_1 is slicing or gating the electron pulse for interaction with the UV pulse (see Fig. 1). We also have interferometry measurements on the optical pulses used in the vanadium dioxide study and find, from a preliminary analysis, including chirp, that the pulse length did not exceed 210 fs. Experiments on silver and ZnO nanowires are in progress to accurately determine the temporal response.

The change in PINEM intensity (Fig. 4*A*) reflects the dielectric response of VO_2 during the phase transition process (Eq. **1**). For negative time delay (before arrival of the pump pulse), the PINEM spectrum intensity remains unchanged, whereas after the pump pulse, the phase transition of the VO_2 nanoparticles takes place, and consequently the dielectric properties (17) of the nanoparticles change owing to the change of the lattice structure during the phase transition. The result is the decay of PINEM intensity after $\tau_2 = 0$ ps that is significant at 20 ps, followed by a slow decay lasting hundreds of picoseconds to about

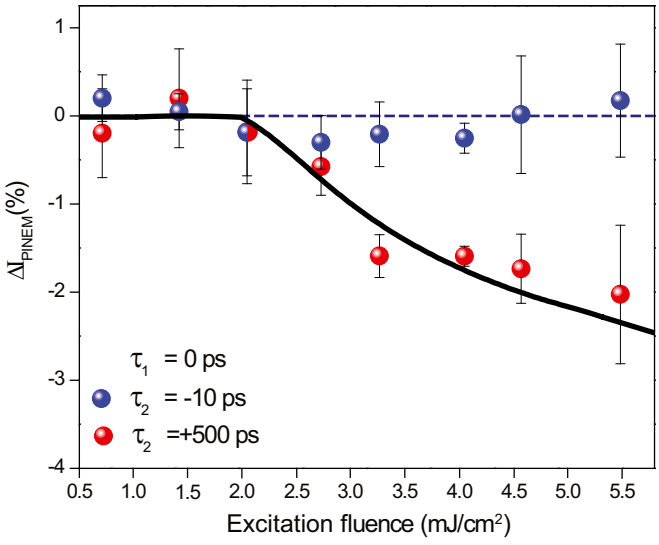

Fig. 5. Fluence dependence of PINEM intensity for the phase transition of vanadium dioxide. Shown are the PINEM intensity change as a function of the excitation fluence at two different delay times of the pump pulse: $\tau_2 = -10$ ps, which is depicted in blue points, and $\tau_2 = +500$ ps, which is shown as red points. The blue dashed line and solid black line are guidelines. The data points present the average integration of five PINEM spectra at the corresponding fluence. The decrease in the PINEM intensity at $\tau_2 = +500$ ps shows the phase transition occurs around a threshold of 2 mJ/cm^2 and increases with fluence (see the text).

PHYSICS

1% total change in PINEM intensity. A biexponential fitting of the PINEM intensity change (red line, Fig. 4*A*) reveals two time constants: first, an ultrafast dynamic (occurring within 10 ps), which is attributed to vanadium atom motion within the unit cell; second, a slower dynamic on the order of ~170 ps, which is attributed to long-range shear rearrangement essential in the rutile phase transformation process. These two distinct processes (30, 33) can be described by an energy landscape (34) as illustrated by Cavalleri (34).

To ensure that the dynamic change of the PINEM intensity, as retrieved from the time-resolved PINEM measurements in Fig. 4*A*, is related to the dynamics of the photoinduced phase transition in VO_2 nanoparticles, we have conducted time-resolved electron diffraction experiments on the same specimen, under the same condition, but with the diffraction pattern being recorded as a function of the second optical (pump) pulse delay (τ_2). The electron diffraction patterns at two different delay times ($\tau_2 = -50$ and +500 ps) are shown in Fig. 4 *B* and *C*, respectively. The diffraction pattern at the negative delay time ($\tau_2 = -50$ ps) shows the Bragg spots 1, 2, 3, and 4, which persist only in the monoclinic (low-temperature) phase of VO_2 (35), and Bragg spot 5, which belongs to the graphene substrate. After the pump pulse (τ_2 = +500 ps), Bragg spots 1, 2, 3, and 4 disappear, which indicates a phase transition of VO_2 from the monoclinic to the tetragonal (rutile) phase, whereas the Bragg spot 5 intensity remains unchanged, indicating that the graphene substrate does not have influence on the measured dynamics depicted in Fig. 3*D* (see the *Supporting Information*, *section S2*).

To investigate the phase transition dynamics, we have traced the intensity change of Bragg spot 2 as it evolves with time (delay τ_2), which is shown in Fig. 4*D*. A fit of this intensity decay (red line, Fig. 4*D*) again reveals two time constants, here on the order of 10 and 140 ps. The pattern indicates a dynamic behavior comparable to that observed in the time-resolved PINEM measurement in Fig. 4*A* and quite similar to results from previous study in this laboratory (30). The results suggest that the photoinduced dielectric response of VO_2 is dominated by its atomic unit cell and lattice arrangements in the phase transition process.

With the reported PINEM technique, we have also studied the excitation fluence dependence of the phase transition in the nanoparticles studied. The first optical pulse (P_1) (1.3 mJ/cm^2) has been set at τ_1=0 ps, with two settings of the second optical (pump) pulse (P_2) at $\tau_2 = -10$ ps and +500 ps, respectively. Then, the change in the intensity of the PINEM spectrum (generated by the coupling of P_1 and electron pulses, Fig. 3*A*) as a function of the excitation pulse fluence was measured at these two time instants. When probing before the arrival of the pump pulse ($\tau_2 = -10$ ps), the PINEM intensity remains nearly constant as the excitation fluence increases, as shown by the blue data points and its dashed guideline in Fig. 5. In contrast, when probing after the pump laser pulse for τ_2 = +500 ps, the PINEM intensity remains unchanged until reaching a certain fluence threshold value near 2 mJ/cm^2, above which the phase transition of the system ensues, with increase in the change, as shown in the red data points and the black guideline in Fig. 5. The low fluence threshold is consistent with the recent study of the same crystalline structure system (36). (More details can be found in *Supporting Information*, *section S3*.)

In conclusion, we have demonstrated a UEM variant, using PINEM probing, but with two optical pulses (instead of one), thus enabling four-dimensional (4D) imaging of dynamics and with optically gated electron pulses. The technique was demonstrated using the nanoscale insulator–metal phase transition of vanadium dioxide. It should now be possible to map dynamics of structures, dielectric response, and charge carriers in other strongly correlated materials. Moreover, this demonstration of using the optical gating of ultrashort electron pulses promises to attain overall temporal resolution in UEM of few femtoseconds and possibly attoseconds for 4D imaging; here, we achieved 3× improvement in temporal resolution by the optical pulses available in our UEM-2.

ACKNOWLEDGMENTS. We thank Dr. S. T. Park for very helpful discussion and Dr. B-K. Yoo for his help in the initial studies of photon-induced near-field electron microscopy (PINEM) on ZnO nanowires. This work was supported by the National Science Foundation Grant DMR-0964886 and the Air Force Office of Scientific Research Grant FA9550-11-1-0055S for research conducted at The Gordon and Betty Moore Center for Physical Biology at the California Institute of Technology.

1. Zewail AH, Thomas JM (2010) *4D Electron Microscopy: Imaging in Space and Time* (Imperial College Press, London).
2. Zewail AH (2014) *4D Visualization of Matter* (Imperial College Press, London).
3. Zewail AH (2010) Four-dimensional electron microscopy. *Science* 328(5975):187–193.
4. Barwick B, Flannigan DJ, Zewail AH (2009) Photon-induced near-field electron microscopy. *Nature* 462(7275):902–906.
5. Park ST, Lin M, Zewail AH (2010) Photon-induced near-field electron microscopy (PINEM): Theoretical and experimental. *New J Phys* 12(12):123028.
6. Park ST, Zewail AH (2014) Photon-induced near-field electron microscopy: Mathematical formulation of the relation between the experimental observables and the optically driven charge density of nanoparticles. *Phys Rev A* 89(1):013851.
7. Howie A (2009) Photon-assisted electron energy loss spectroscopy and ultrafast imaging. *Microsc Microanal* 15(4):314–322.
8. de Abajo FG, Kociak M (2008) Electron energy-gain spectroscopy. *New J Phys* 10(7): 073035.
9. Yurtsever A, van der Veen RM, Zewail AH (2012) Subparticle ultrafast spectrum imaging in 4D electron microscopy. *Science* 335(6064):59–64.
10. Piazza L, et al. (2015) Simultaneous observation of the quantization and the interference pattern of a plasmonic near-field. *Nat Commun* 6:6407.
11. Park ST, Yurtsever A, Baskin JS, Zewail AH (2013) Graphene-layered steps and their fields visualized by 4D electron microscopy. *Proc Natl Acad Sci USA* 110(23): 9277–9282.
12. Kirchner FO, Gliserin A, Krausz F, Baum P (2014) Laser streaking of free electrons at 25 keV. *Nat Photonics* 8(1):52–57.
13. Plemmons DA, Tae Park S, Zewail AH, Flannigan DJ (2014) Characterization of fast photoelectron packets in weak and strong laser fields in ultrafast electron microscopy. *Ultramicroscopy* 146(0):97–102.
14. Flannigan DJ, Barwick B, Zewail AH (2010) Biological imaging with 4D ultrafast electron microscopy. *Proc Natl Acad Sci USA* 107(22):9933–9937.
15. Park ST, Zewail AH (2012) Enhancing image contrast and slicing electron pulses in 4D near field electron microscopy. *Chem Phys Lett* 521(0):1–6.
16. Corkum P, Krausz F (2007) Attosecond science. *Nat Phys* 3(6):381–387.
17. Lysenko S, Vikhnin V, Fernandez F, Rua A, Liu H (2007) Photoinduced insulator-to-metal phase transition in VO_2 crystalline films and model of dielectric susceptibility. *Phys Rev B* 75(7):075109.
18. Dicken MJ, et al. (2009) Frequency tunable near-infrared metamaterials based on VO_2 phase transition. *Opt Express* 17(20):18330–18339.
19. Cilento F, et al. (2010) Ultrafast insulator-to-metal phase transition as a switch to measure the spectrogram of a supercontinuum light pulse. *Appl Phys Lett* 96(2):021102.
20. Rini M, et al. (2008) Optical switching in VO_2 films by below-gap excitation. *Appl Phys Lett* 92(18):181904.
21. Cavalleri A, et al. (2001) Femtosecond structural dynamics in VO_2 during an ultrafast solid-solid phase transition. *Phys Rev Lett* 87(23):237401.
22. Berglund CN, Guggenheim HJ (1969) Electronic proerties of VO_2 near semiconductor-metal transition. *Phys Rev* 185(3):1022.
23. Morin FJ (1959) Oxides which show a metal-to-insulator transition at the Neel temperature. *Phys Rev Lett* 3(1):34–36.
24. Petrov GI, Yakovlev VV, Squier JA (2002) Nonlinear optical microscopy analysis of ultrafast phase transformation in vanadium dioxide. *Opt Lett* 27(8):655–657.
25. Hada M, et al. (2012) Hot electron injection driven phase transitions. *Phys Rev B* 86(13):134101.
26. Kübler C, et al. (2007) Coherent structural dynamics and electronic correlations during an ultrafast insulator-to-metal phase transition in VO_2. *Phys Rev Lett* 99(11):116401.
27. Jepsen PU, et al. (2006) Metal-insulator phase transition in a VO_2 thin film observed with terahertz spectroscopy. *Phys Rev B* 74(20):205103.
28. Cavalleri A, et al. (2005) Band-selective measurements of electron dynamics in VO_2 using femtosecond near-edge x-ray absorption. *Phys Rev Lett* 95(6):067405.
29. Cavalleri A, Rini M, Schoenlein RW (2006) Ultra-broadband femtosecond measurements of the photo-induced phase transition in VO_2: From the mid-IR to the hard X-rays. *J Phys Soc Jpn* 75(1):011004.
30. Baum P, Yang D-S, Zewail AH (2007) 4D visualization of transitional structures in phase transformations by electron diffraction. *Science* 318(5851):788–792.
31. Lobastov VA, Weissenrieder J, Tang J, Zewail AH (2007) Ultrafast electron microscopy (UEM): Four-dimensional imaging and diffraction of nanostructures during phase transitions. *Nano Lett* 7(9):2552–2558.
32. Zewail AH, Lobastov V (2006) Method and system for ultrafast photoelectron microscope. US Patent 7,154,091 B2, 20050401.
33. Kucharczyk D, Niklewski T (1979) Accurate X-ray determination of the lattice parameters and the thermal expansion coefficients of VO_2 near the transition temperature. *J Appl Cryst* 12(4):370–373.

34. Cavalleri A (2007) Chemistry. All at once. *Science* 318(5851):755–756.
35. Liu H, Kwon O-H, Tang J, Zewail AH (2014) 4D imaging and diffraction dynamics of single-particle phase transition in heterogeneous ensembles. *Nano Lett* 14(2): 946–954.
36. Morrison VR, et al. (2014) A photoinduced metal-like phase of monoclinic VO_2 revealed by ultrafast electron diffraction. *Science* 346(6208):445–448.
37. Chae B-G, et al. (2006) Highly oriented VO_2 thin films prepared by sol-gel deposition. *Electrochem Solid-State Lett* 9(1):C12–C14.
38. Kana Kana JB, Ndjaka JM, Vignaud G, Gibaud A, Maaza M (2011) Thermally tunable optical constants of vanadium dioxide thin films measured by spectroscopic ellipsometry. *Opt Commun* 284(3):807–812.
39. Fu D, et al. (2013) Comprehensive study of the metal-insulator transition in pulsed laser deposited epitaxial VO_2 thin films. *J Appl Phys* 113(4):043707.
40. Kakiuchida H, Jin P, Nakao S, Tazawa M (2007) Optical properties of vanadium dioxide film during semiconductive–metallic phase transition. *Jpn J Appl Phys* 46 (2L):L113.
41. Kang MI, et al. (2012) Dependence of optical properties of vanadium oxide films on crystallization and temperature. *Thin Solid Films* 520(6):2368–2371.
42. Verleur HW, Barker A, Jr, Berglund C (1968) Optical properties of VO_2 between 0.25 and 5 eV. *Phys Rev* 172(3):788.
43. Leroux C, Nihoul G, Van Tendeloo G (1998) From VO_2 (B) to VO_2 (R): Theoretical structures of VO_2 polymorphs and in situ electron microscopy. *Phys Rev B* 57(9):5111.
44. Oh D-W, Ko C, Ramanathan S, Cahill DG (2010) Thermal conductivity and dynamic heat capacity across the metal-insulator transition in thin film VO_2. *Appl Phys Lett* 96(15):151906.